DOI: 10.13009/EUCASS2022-7247
9TH EUROPEAN CONFERENCE FOR AERONAUTICS AND SPACE SCIENCES (EUCASS)

Effect of Recess Length on Combustion Characteristics of Additive Manufactured Swirl Coaxial Injector

Cheolwoong Kang, Shinwoo Lee*, Sun Woo Han*, Kangyeong Lee*, Hadong Jung*, Kyubok Ahn*, Ha Young Lim**, and Byoungjik Lim****

**School of Mechanical Engineering, Chungbuk National University*

Chungdae-ro 1, Seowon-Gu, Cheongju, Chungbuk 28644, Korea

***Launcher Propulsion Control Team, Korea Aerospace Research Institute*

169-84, Gwahak-ro, Yuseong-Gu, Daejeon, 34133, Korea

****Small Launcher R&D Office, Korea Aerospace Research Institute*

169-84, Gwahak-ro, Yuseong-Gu, Daejeon, 34133, Korea

Abstract

In this study, additive manufacturing was applied to manufacture a new manifold cooled by an oxidizer and the internal structure of an injector that is difficult to implement with machining. The injector head is manufactured by SLM (Selective Laser Melting) method using UNS S31603 single material. In order to confirm the combustion characteristics according to the length of the recess, hot-firing tests were performed on three injectors having different lengths of the recess. In addition, the structural/thermal stability of the injector head made of additive manufacturing and UNS S31603 was verified.

1. Introduction

The space launch vehicle field is rapidly changing with the advancement of private companies such as Space X, Blue Origin, Launcher, Rocket Lab, and Additive Rocket Corporation. Recently, the key of the space launch vehicle field is to reduce the cost of manufacturing and operating the launch vehicle. For this purpose, additive manufacturing called 3D printing is being applied. The biggest advantage of using additive manufacturing is the flexibility of manufacturing. A product having a complex structure and a product composed of multiple parts can be manufactured into one integrated product. In addition, the recent improvement in quality due to the development of additive manufacturing technology makes it possible to apply additive manufacturing to projectile manufacturing. Superdraco, Rutherford, E-2, Prometheus, Vulcain 2.1, Vinci, M10, KRE-007, and LE-9 engines are rocket engines being built and developed using additive manufacturing [1-6].

PBF (Powder Bed Fusion) and DED (Directed Energy Deposition) are representative methods for additive manufacturing of metals. The PBF method is to melt and bond the metal powder by injecting a heat source such as a laser beam into the metal powder placed on the bed. On the other hand, DED is a method that melts and deposits a material by applying thermal energy to a metal wire or powder supplied through a nozzle. The DED method allows for rapid manufacturing, and the large chamber of the DED allows for the creation of large structures. The disadvantage is that the surface roughness is bad. PBF has a slow manufacturing speed and is not suitable for manufacturing large structures because the printer chamber is small. However, PBF has the advantage of having better surface roughness than DED. In this regard, PBF is mainly applied to the manufacture of rocket engine parts, and most of the engines mentioned above have also been applied with the PBF method [7-8].

The thrust chamber of a liquid rocket engine consists of an injector head part and a combustion chamber part. The injector head is divided into a manifold and an injector. Methane engines have similarities to hydrogen engines that use cryogenic fuel. In most hydrogen engines, the cryogenic oxidizer flows into the manifold dome, and hydrogen is supplied to the bottom manifold. Hydrogen fed to the lower manifold cools the faceplate of the manifold. In addition, transpiration cooling is sometimes applied by making faceplates from porous materials due to the low heat transfer of gaseous hydrogen [9-10]. The atomization and mixing performance of the injectors that supply propellant to the combustion chamber directly affect the combustion performance of the rocket engine. Therefore, selecting the appropriate injector according to the propellant combination and the engine's mission is important. In liquid rocket engines that use bipropellants, injectors are generally divided into coaxial injectors, impingement injectors, and pintle injectors. Liquid/gas propellant combinations often use coaxial injectors, in which the oxidizer and fuel are injected

DOI: 10.13009/EUCASS2022-7247

with the same axis. The coaxial injector has the advantage of excellent atomization performance and combustion stability. Coaxial injectors are affected by geometrical parameters such as recess length and taper angle [11].
As the application of additive manufacturing increases in the space launch vehicle field, the Korea Aerospace Research Institute plans to apply the SLM method to the production of 1-tonf methane engines. To confirm in advance the combustion characteristics and structural stability of the thrust chamber head to be manufactured by the SLM method, a uni-element thrust chamber head was preferentially additive manufactured. The hot-firing test of the additively manufactured uni-element thrust chamber head was conducted at the 1kN-class methane engine combustion test facility of Chungbuk National University. By taking advantage of the advantages of additive manufacturing, a manifold with a complex shape injector and oxidizing agent is supplied to the lower manifold to cool the faceplate was fabricated. UNS S31603 single material is used, which is cheaper than Inconel alloy. Hot-firing tests were performed to confirm the combustion characteristics and structural/thermal stability of the initially manufactured injector head. In addition, to confirm the effect of the recess length on the combustion characteristics, combustion tests of injectors with different recess lengths were also performed. For injectors with different recess lengths, electric discharge machining was performed on the initially manufactured injectors.

2. Uni-element thrust chamber and test condition

The model 1-tonf methane engine uses 18 injectors. To verify the design of the injector and manifold through a hot-firing test before production of the actual model, a uni-element thrust chamber head with one injector was designed and manufactured through additive manufacturing. Fig. 1 is a schematic diagram of a uni-element thrust chamber, and the performance specifications under the design point conditions are summarized in Table 1. A uni-element thrust chamber consists of an injector head (injector and manifold), a combustion chamber cylinder part, and a nozzle part, each of which is coupled with bolts, nuts, and copper gaskets.

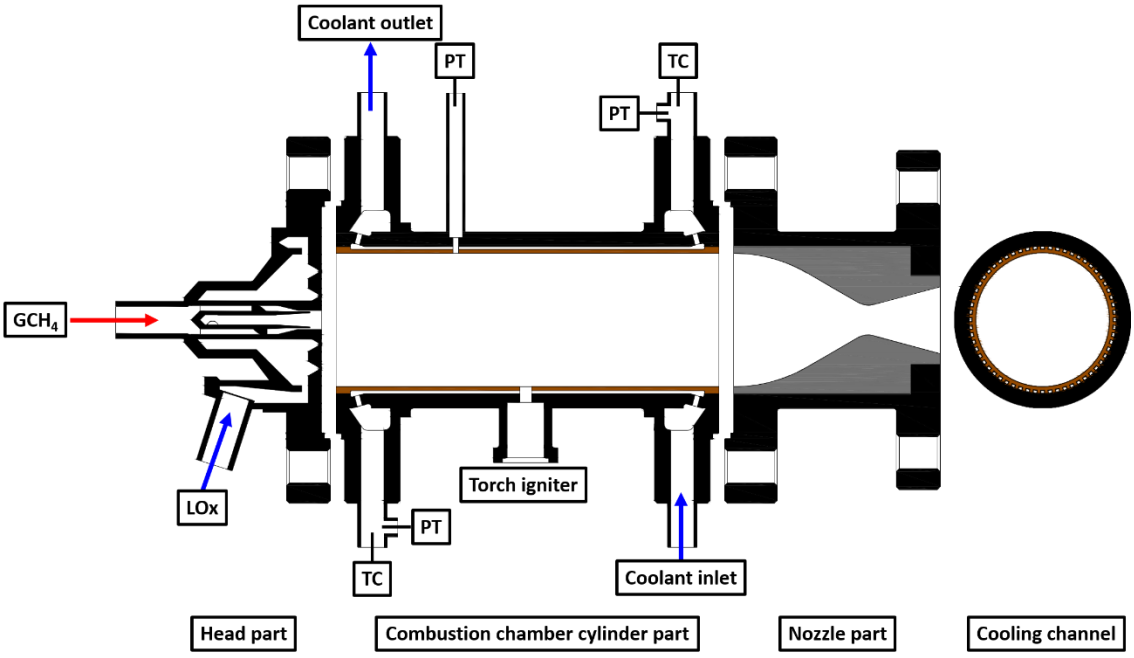

Figure 1: Schematic of the uni-element thrust chamber

Table 1: Uni-element thrust chamber specification

Parameter	Value
F_{vac} [N]	545
P_c [bar]	35
O/F ratio	3.00
$\dot{m}_t$ [g/s]	161.6

DOI: 10.13009/EUCASS2022-7247

2.1 Injector head

In most liquid rocket engines, the manifold faceplate is cooled with fuel such as kerosene, hydrogen, or methane, and the faceplate is sometimes made of porous material. However, the manifold in this study was cooled through a cryogenic oxidizer. Fig. 2 is a cross-section of the manufactured manifold, showing the supply method of the oxidizer and fuel. Liquid oxygen supplied to the manifold is fed to the injector after cooling the faceplate, and gaseous methane is directly injected into the combustion chamber.
An expander closed cycle is applied to the methane engine, which becomes a actual model. In the case of the expander cycle, cryogenic liquid hydrogen and liquid methane are used as fuels. The cryogenic fuel cools the hot thrust chamber as it passes through the cooling channels of the thrust chamber. The fuel vaporized through the heat from the thrust chamber is fed to the turbine and injector head. Therefore, the propellant is injected as a liquid/gas propellant combination [12]. The injector manufactured for the hot-firing test is a coaxial injector with proven combustion performance and stability in liquid/gas propellant combinations. Fig. 3 shows a cross-section of the manufactured injector. The oxidizer is fed through a tangential hole in the central oxidizer injector and swirled, while the fuel is swirled through the vanes of the injector and injected annularly around the oxidizer. Table 2 shows the design parameters and values of the injector. The initially manufactured injector (Inj#A) had a recess length of 0 mm and a taper angle of 7.5°. After the hot-firing tests, the recess lengths were modified to 2 mm (Inj#B) and 4 mm (Inj#C) through electric discharge machining.

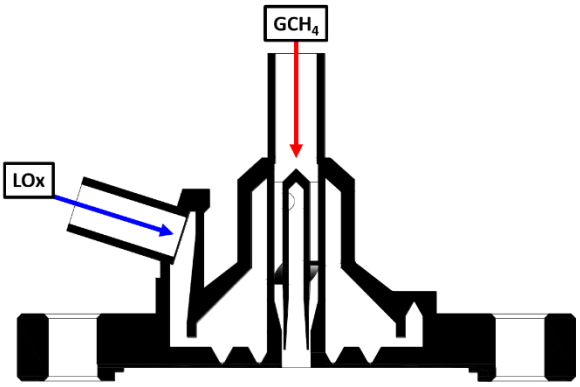

Figure 2: Schematic of the injector head

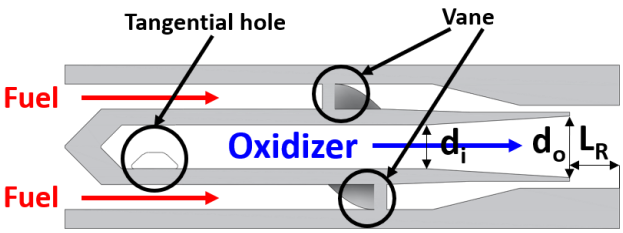

Figure 3: Schematic of the injector

Table 2: Design parameters of the injectors

	Inj#A	Inj#B	Inj#C
Parameter	**Value**		
L_R [mm]	0.0	2.0	4.0
d_i [mm]	3.5		
d_o [mm]	4.9		

The injector and manifold are integrated products manufactured by SLM (Selective Laser Melting) method, and UNS S31603 single material is used. Fig. 4 shows the manufactured manifold and injector. The flange for connecting the injector head and combustion chamber was manufactured through machining, and the manifold and flange were joined through tig welding. The injector can be seen in the picture on the right of Fig. 4.

DOI: 10.13009/EUCASS2022-7247

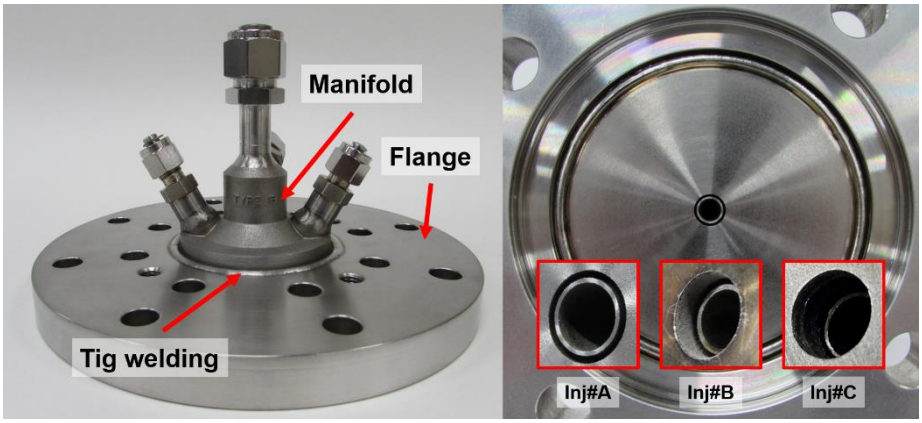

Figure 4: Photograph of the injector head

2.2 Combustion chamber part

The combustion chamber consists of a cylinder part and a nozzle part, both of which are machined. The cylinder part simulates the regenerative cooling type, and the cooling channel is machined. The inner wall of the cylinder is made of copper alloy material, and the outer jacket is made of UNS S31803 material. In addition, the outer jacket and inner wall were joined by brazing. Fig. 1 shows the schematic diagram of the cylinder part. The inner diameter of the cylinder is 45.75 mm, and the length from the faceplate to the nozzle throat is 177.38 mm. In the cylinder part, the internal pressure (PT) of the combustion chamber and the temperature (TT) and pressure (PT) of the inlet/outlet of the cooling channel can be measured. Also, since the main propellant is ignited by the torch igniter, the port for installing the torch igniter has been machined. The nozzle part has a nozzle throat diameter of 10.23 mm, and the inside is made of graphite material by applying ablation cooling. The housing of the nozzle part is made of UNS S31603 material to withstand the combustion pressure.

2.3 Condition of hot-firing test

The mixture ratio condition of the hot-firing test is 3.0, which is the design point of a 1-tonf methane engine. The propellant mass flow rate reflects the change in the number of injectors from 18 to uni-element. However, considering that the injector head is the first prototype by additive manufacturing, the combustion chamber pressure was set to 25 bar instead of the target pressure of 35 bar. Table 4 shows the nominal conditions of combustion chamber pressure, propellant mass flow, and mixture ratio. In addition to the nominal condition, hot-firing tests were performed in various ranges by increasing or decreasing the mixture ratio.

Table 3: Nominal condition of the hot-firing test

Parameter	Specification
Propellant	LOx/GCH$_4$
P_c [bar]	25
O/F ratio	3.00
$\dot{m}_t$ [g/s]	115.74

3. Results

Hot-firing tests of methane engine uni-element thrust chamber have been performed a total of 30 times at the 1 kN-class methane engine combustion test facility at Chungbuk National University. The hot-firing test equipment, control system, measurement system, and hot-firing test method are described in detail in the paper of Kang et al. [13].
Fig. 5 shows a snapshot of the hot-firing test. The combustion chamber pressure according to the mixture ratio resulting from the hot-firing test is shown in Fig. 6. The hot-firing tests for A, B, and C injectors were performed 13 times, 11 times, and six times. In the hot-firing tests of the C injector, the nozzle throat was rapidly abraded, and only six times were performed.

DOI: 10.13009/EUCASS2022-7247

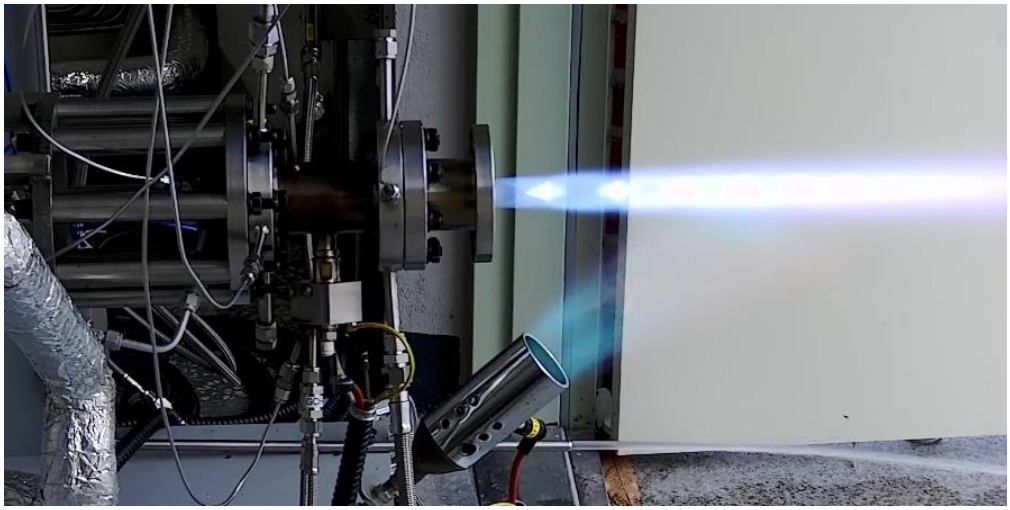

Figure 5: Snapshot of the hot-firing test

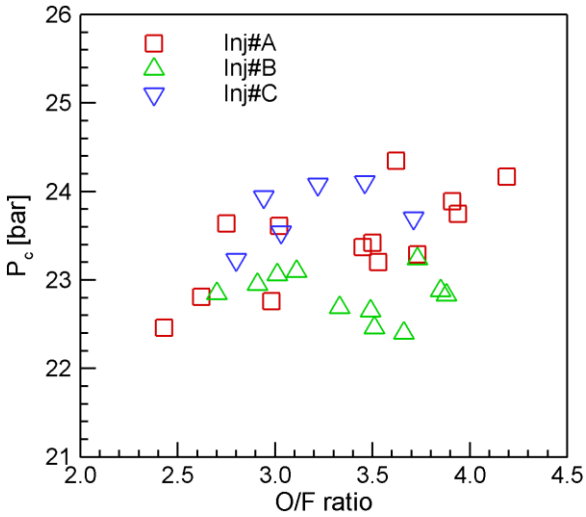

Figure 6: Combustion chamber pressure of the hot-firing tests

Fig. 7 shows the mass flow rate of the propellant, the combustion chamber pressure, the propellant temperature at the manifold, and the coolant temperature at the cooling channel inlet/outlet as a result of the hot-firing test. The pressure in the 4 to 7-second section is the combustion pressure of the torch igniter used to ignite the main propellant. It can be seen that the main propellant is supplied at 8 seconds and the combustion chamber pressure rises rapidly. After about 18 seconds, the main propellant was shut down, and the hot-firing test was finished. There is no difference in the coolant temperature at the inlet and outlet of the cooling channel before the main propellant is burned. The main propellant is burned, and the difference in coolant temperature at the inlet and outlet of the cooling channel occurs. Data excluding dynamic pressure are averaged over a 0.2-second section indicated by a black dotted line.

DOI: 10.13009/EUCASS2022-7247

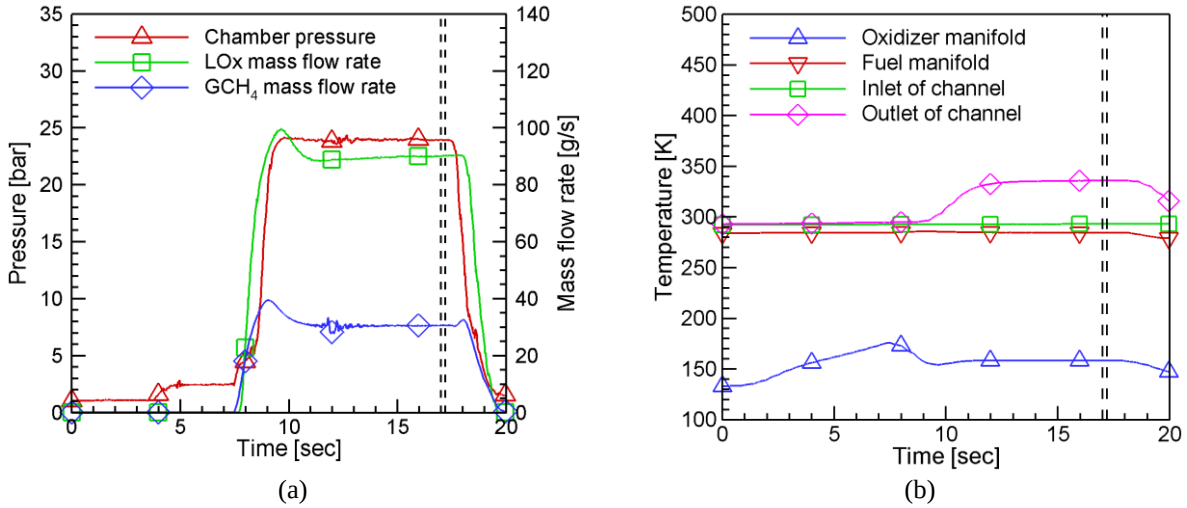

(a) (b)

Figure 7: Result of the hot-firing test, where (a) is mass flow rate and combustion pressure and (b) is temperature of the propellant and coolant

3.1 Combustion characteristics

Rocket engine performance is mainly judged by specific impulse, and thrust measurement is required to obtain specific impulse. Since combustion performance is a concern of this study, a nozzle with a small nozzle expansion ratio was used. Therefore, the characteristic velocity efficiency (η_{c^*}) was used as the criterion of combustion performance, and the combustion characteristic velocity (c^*) and characteristic velocity efficiency were obtained and confirmed. The experimental combustion characteristic velocity (c^*_{exp}) in the hot-firing test is calculated from Eq. 1. Combustion chamber pressure (P_c) and total propellant mass flow rate ($\dot{m}_t$) are averages of the data measured during the hot-firing test. The nozzle throat area (A_t) was calculated as the average value of the nozzle throat diameters measured with a micrometer before and after the hot-firing test. The combustion characteristic velocity efficiency is the experimental combustion characteristic velocity compared to the theoretical combustion characteristic velocity (c^*_{idel}) as in Eq. 2. The theoretical combustion characteristic velocity was obtained by inputting hot-firing test data into the RPA program, which is a commercial program. The cylinder part is cooled by the coolant passing through the cooling channel. As shown in Fig. 1, the coolant is supplied from the downstream of the cylinder opposite to the flow direction of the combustion gas and discharged upstream. Water was used as the coolant, and the heat flux was calculated to confirm the cooling performance. The heat flux is calculated through Eq. 3. In calculating the heat flux, the average values of the temperature and pressure of the coolant measured at the inlet and outlet of the cooling channel were used for the specific heat at constant pressure (c_p). Also, the temperature change (ΔT) is the temperature difference between the outlet and the inlet of the cooling channel, and A_{cyl} is the inner area of the cylinder.

$$c^* = (P_c \times A_t)/\dot{m}_t \quad \textbf{(1)}$$

$$\eta_{c^*} = c^*_{exp}/c^*_{idel} \quad \textbf{(2)}$$

$$\ddot{q} = (\dot{m}_c \times c_p \times \Delta T)/A_{cyl} \quad \textbf{(3)}$$

Fig. 8 shows the experimental and theoretical combustion characteristics velocity with the mixture ratio. Comparing the experimental combustion velocity of Inj#A and Inj#B, the recess length increased by 2 mm, but the performance was not improved. On the other hand, it is confirmed that the combustion characteristic velocity of Inj#C is improved than that of Inj#A and Inj#B. Fig. 9 shows the combustion characteristic velocity efficiency of the three injectors, and the dotted line is the average combustion characteristic velocity efficiency for each injector. It is confirmed that the average combustion characteristic velocity efficiency is also high as Inj#C is improved in the experimental combustion characteristic velocity. When the recess length and the oxidizer outlet diameter are similar, the atomization and mixing performance is improved, which is also related to the combustion efficiency [14]. Therefore, it is judged that the combustion efficiency of Inj#C, which has a similar oxidizer outlet diameter and recess length, is improved compared to Inj#A and Inj#B.

DOI: 10.13009/EUCASS2022-7247

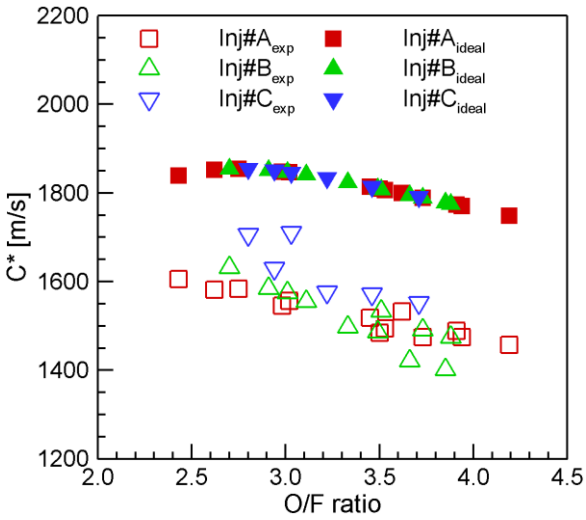

Figure 8: Characteristic velocity with O/F ratio

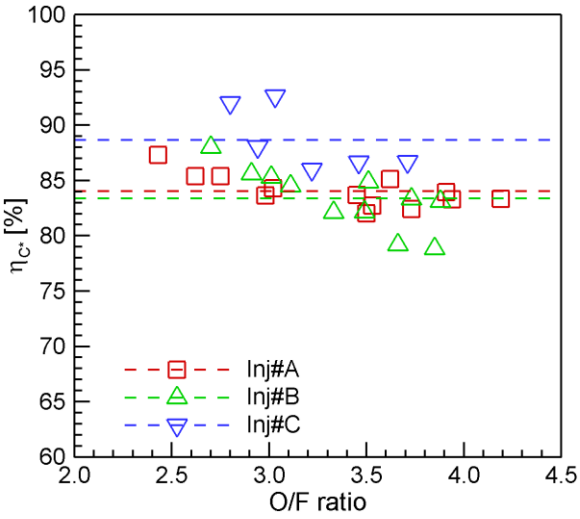

Figure 9: Characteristic velocity efficiency with O/F ratio

Fig. 10 is the heat flux result according to the mixture ratio, and the dotted line is the average heat flux for each injector. The average heat flux is high in Inj#C. The combustion performance was improved by internal mixing in the recess area. Therefore, Inj#C, which has the longest recess length, has the largest heat flux.

DOI: 10.13009/EUCASS2022-7247

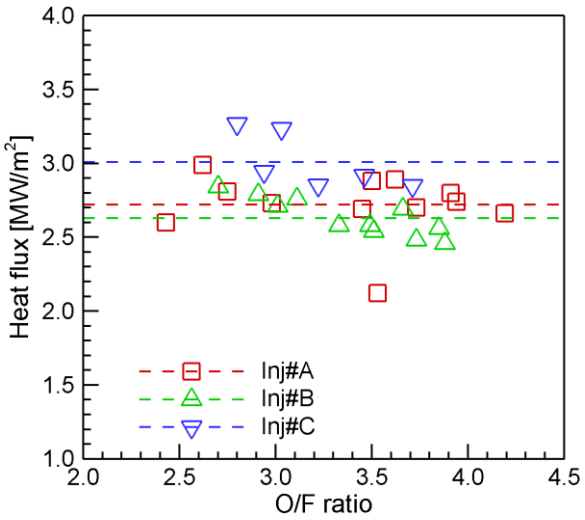

Figure 10: Heat flix with O/F ratio

The dynamic pressure generated during combustion upstream of the fuel manifold was measured. Dynamic pressure measured at 10,000 Hz was subjected to FFT analysis by bandpass filtering in the section of about 30 Hz to 4,999 Hz. Fig. 11(a) and Fig. 11(b) is the filtered dynamic pressure data when the pressure fluctuation is small and large, respectively. The ignition of the main propellant causes the big pick at 8 seconds. After that, it can be confirmed that the dynamic pressure of the hot-firing test with small pressure fluctuations does not develop. In the case of the hot-firing test with large fluctuations, the main propellant is ignited, and the fluctuations gradually increase linearly. Fig. 12 shows the RMS value of the pressure fluctuation versus the combustion chamber pressure of Inj#B and Inj#C. The value with the maximum RMS value of the pressure fluctuation relative to the combustion chamber pressure is 0.41%. It is judged that all combustion tests were carried out stably with less than 3%, which is the criterion for combustion instability.

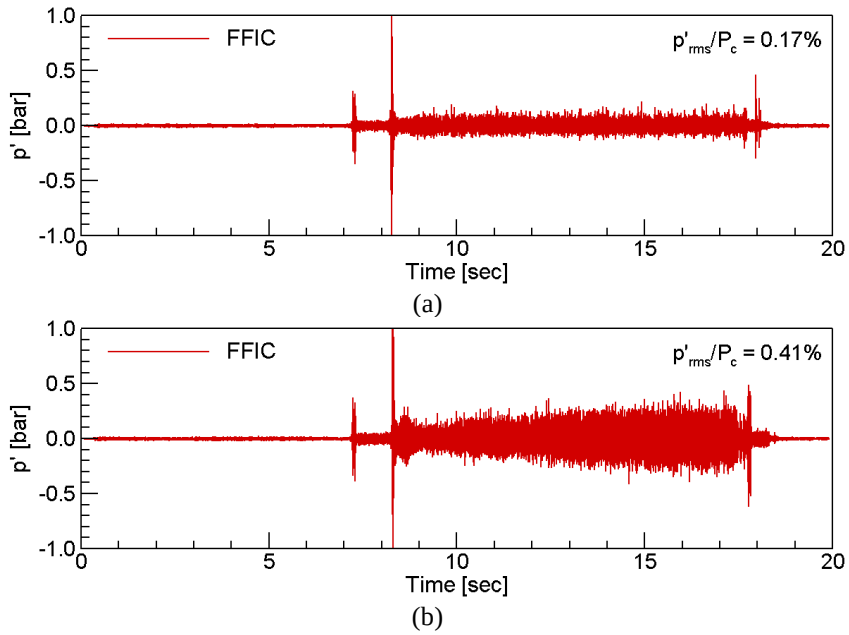

Figure 11: Filtered dynamic pressure, where (a) is small pressure fluctuation and (b) is large pressure fluctuation

DOI: 10.13009/EUCASS2022-7247

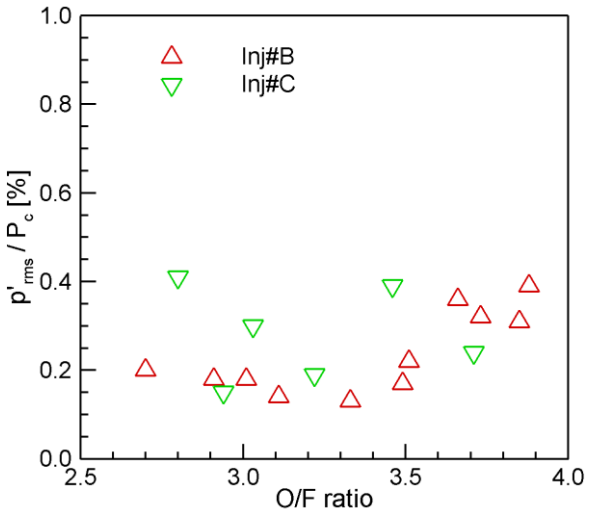

Figure 12: p'_{rms}/P_c with O/F ratio

3.2 Condition of the injector head

The injector head manufactured additively using UNS S31603 single material has a cumulative burn time of 300 seconds. Fig. 13 shows the faceplate and internal injectors of the manifold before and after the hot-firing test. Although a method cooled by a cryogenic oxidizer was applied instead of the generally applied faceplate cooling method, no damage to the faceplate of the injector head and the injector was confirmed even after the hot-firing test.

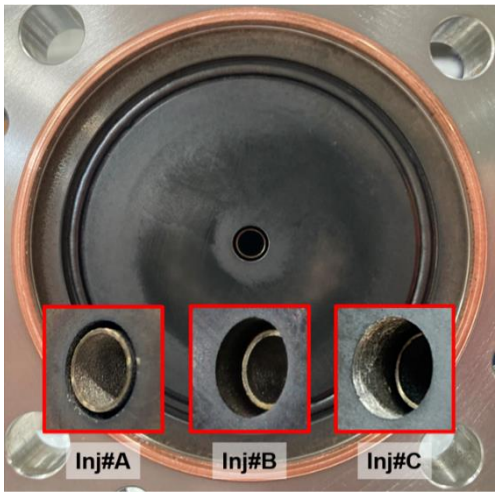

Figure 13: Photograph of the injector head after hot-firing tests

4. Conclusion

Additive manufacturing was applied to manufacture a new manifold cooled by an oxidizer and the internal structure of an injector that is difficult to implement with machining. The injector head is manufactured by SLM (Selective Laser Melting) method using UNS S31603 single material. The combustion characteristics and structural/thermal stability of the initially manufactured injector head were confirmed. Also, the combustion characteristics according to the length of the recess were confirmed. It was confirmed that the combustion efficiency and heat flux were high in the injector with the longest recess length. All hot-firing tests were performed stably without combustion instability. The injector head cooled by the cryogenic oxidizer was not damaged even with a cumulative combustion time of 300 seconds.

DOI: 10.13009/EUCASS2022-7247

References

[1] Kerstens, F., A. Cervone, and P. Gradl. 2021. End to end process evaluation for additively manufactured liquid rocket engine thrust chambers. Acta Astronaut. 182:454-465.

[2] Kumar, L.J., and C.G. Nair. 2017. Current trends of additive manufacturing in the aerospace industry. Advances in 3D printing & additive manufacturing technologies. Springer.

[3] Iannetti, A., N. Girard, D. Tchou-kien, C. Bonhomme, N. Ravier, and E. Edeline. 2017. Prometheus, a LOx/LCH_4 reusable rocket engine. In: 7th European Conference for Aeronautics and Space Sciences. 39-54.

[4] Kajan D., D. Liuzzi, C. Boffa, M. Rudnykh, D. Drigo, L. Arione, N. Ierardo, and A. Sirbi. 2019. Development of the liquid oxygen and methane M10 rocket engine for the Vega-E upper engine. In: 8th European Conference for Aeronautics and Space Sciences.

[5] Lee, K.O., B. Kim, D.J. Kim, M. Hong, and K. Lee. 2020. Technology trends in additively manufactured small rocket engines for launcher applications. KSPE Journal. 24(2):73-82.

[6] Kawashima, H., Y. Funakoshi, A. Kurosu, T. Kobayashi, and K. Okita. 2019. Development status of LE-9 engine for H3 launch vehicle. In: AIAA Propulsion and Energy.

[7] Yap, C.Y., C.K. Chua, Z.L. Dong, Z.H. Liu, D.Q. Zhang, L.E. Loh, and S.L. Sing. 2015. Review of selective laser melting: materials and applications. Appl Phys Rev. 2(4):041101.

[8] Blakey-Milner, B., P. Gradl, G. Snedden, M. Brooks, J. Pitot, E. Lopez, F. Berto, and A. Du Plessis. 2021. Metal additive manufacturing in aerospace: A review. Materials & Design. 209:110008.

[9] Lux, J., D. Suslov, and O. Haidn. 2008. On porous liquid propellant rocket engine injectors. Aerosp Sci and Technol. 12(6):469-477.

[10] Greuel, D., J. Deeken, and D. Suslov. 2013. Test facilities for SCORE-D. CEAS Space J. 4(1):55-59.

[11] Huzel, D.K., and D.H. Huang. 1992. Mordern engineering for designe of liquid-propellant rocket engines. Progress in Astronautics and Aeronautics. AIAA.

[12] Ukai, S., K. Sakaki, Y. Ishikawa, H. Sakaguchi, and S. Ishihara. 2019. Component tests of a LOX/methane full-expander cycle rocket engine: Injector and regenerative cooled combustion chamber. In: 8th European Conference for Aeronautics and Space Sciences.

[13] Kang, C., D. Hwang, J. Ahn, J. Lee, D. Lee, and K. Ahn. 2021. Methane engine combustion test facility construction and preliminary tests. KSPE Journal. 25(3):88-100.

[14] Saffell, R.J., and M.D. Moser. 2008. GOX/Methane injector effects on combustion efficiency. In: 44th AIAA/ASME/SAE/ASEE Joint Propulsion Conference and Exhibit.